COMPUTER-AIDED DESIGN & APPLICATIONS, 2017
VOL. 14, NO. 6, 760–769
https://doi.org/10.1080/16864360.2017.1287678

Mesoscale geometric modeling of cellular materials for finite element analysis

Michele Bici, Francesca Campana and Micaela De Michelis

Sapienza Università di Roma, Italy

ABSTRACT

Mesoscale geometric modeling of cellular materials is not strictly related only to tomography reconstruction, but it can be applied also in Finite Element Analysis: (a) to better understand load distribution at the interfaces; (b) to develop and calibrate material models; (c) for sensitivity analysis to different loads or shape parameters. This paper aims to examine some of the most applied techniques for geometric modeling of cellular materials at a mesoscale level discussing their advantages and disadvantages for Finite Element Analysis. Among them, two of the most applied techniques, the Voronoi approach and the reverse engineering reconstruction, are here applied to simulate the behavior of aluminum foams under compression. These applications compared to some experimental evidences confirm the capability of mesoscale analysis, highlighting possible enhancement of the geometric modeling techniques.

KEYWORDS

Cellular materials; Finite Element Analysis; Voronoi Diagram; Representative Volume Element; Reverse Engineering

1. Introduction

Cellular materials range from metallic to biological applications. They consist with a non-homogeneous structure defined by pores or voids, named also cells, which are distributed with different shape and dimension. According to [7], "porous materials" have a bulk matrix with small pores in an amount of less than 30-40% while "cellular materials" have a larger amount of voids. Generally speaking, they can be classified according to the cells distribution: thus they can be regular distributed cells or stochastic; open or closed cells; polyhedral or elliptical. Regular distributed cells are organized in a repeated structure of identical cells or sets of them, the distribution can be modeled through a mathematical algorithm. On the contrary, a stochastic distribution can be formed by cells, regular or not, placed randomly. Open cells are connected to each other forming a network. Closed cells are not interconnected and they can allow a higher compressive strength than the open ones, due to their structure. In general, they have a higher density, higher regularity and higher dimensional stability. From the geometric point of view, cells can be polyhedral, if formed by polygonal faces, or elliptical (spherical or similar) if there are no edges and the cell is approximately axial symmetric in one or two directions.

Honeycomb and lattice structure are two examples of regular distributed cells. The first one is an open structure closed by two laminated panels (sandwich structure), the second one defines an open structure (Fig. 1(a). and Fig. 1(b).). They allow weight reduction without drop of stiffness and strength so that they are applied as structural panels in aeronautical applications or bumpers. Metallic foams made by powder technology represent stochastic closed cells. Typically, they are rather spherical or elliptical as shown in Fig. 1(c). On the contrary, foaming through infiltration in a salt pattern produces open cells structures that can be extremely small (pore size is related to salt granulometry), and may assume polyhedral shapes as shown in Fig. 1(d).

Geometric modeling must face different problems considering what it has to accomplish. Two geometric modeling scenarios may be defined: one is related to the reconstruction from direct experimental acquisition (e.g. X-ray tomography or metallographic cross sections), the second one concerns with numerical generation of the virtual model from registered data.

Reconstruction from direct experimental acquisition is derived from medical practice and it is common in bioengineering. In this case, material cells (of both bone and metallic component) have length ranging from 1 to 5 mm

CONTACT Michele Bici michele.bici@uniroma1.it; Francesca Campana francesca.campana@uniroma1.it;
Micaela De Michelis demichelis.1607483@studenti.uniroma1.it

This article was originally published with errors. This version has been corrected/amended. Please see Erratum/Corrigendum (http://dx.doi.org/10.1080/16864360.2017.1300445).

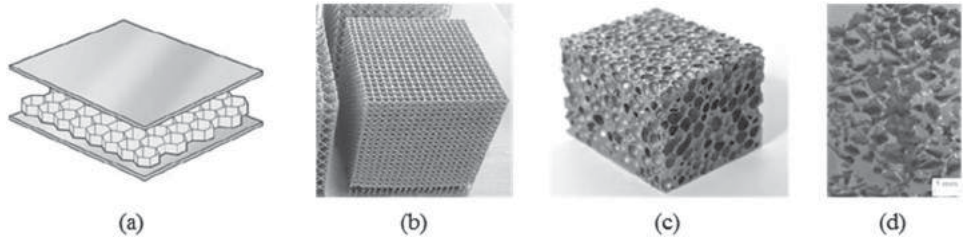

Figure 1. Examples of cellular materials: (a) honeycomb; (b) lattice structure; (c) metallic foam by compact powder; (d) metallic foam by infiltration.

and are distributed according to load paths [11], thus direct acquisition is required to capture the specific test case related to the patient. The same approach has been applied also to mechanical investigation of metallic foams [7]. Since void density and morphology has been demonstrated as the leading parameters of mechanical response, tomography reconstructions have been made to quantify foam's porosity and to investigate its mechanical behavior via FEA.

From the design point of view, this approach is not effective because it requires the experimental investigation on the materials thus the second geometric modeling scenario (numerical generation from registered data) seems to be the most appropriate. In this case, some hypothesis about cell shape and size distribution are made according to experimental observations, then, a pattern of voids is generated and subtracted to the bulk materials. Doing so both regular pattern and stochastic distribution can be made according to the hypothesis applied.

In both scenarios, many difficulties have been faced and discussed in literature. In the reconstruction from direct experimental acquisition, main problems concern with: (a) data acquisition and image analysis post-processing, (b) surface/volume discretization. In numerical generation from registered data, they mainly concern with: (a) the consistency of the assumption related to cell shape and (b) the ability of reproducing the actual stochastic variability of the voids, which is intrinsically due to the manufacturing process. In all cases, the final result (STL, surface or FEA model) may be derived according to the specific aim of the research, often requiring large model processing and checking.

This paper aims to compare the geometric modeling strategies in the respect of the reliability of their virtual prototyping. In Section 2 and 3 the modeling strategies are described and compared, then in Section 4 two test cases are presented, highlighting geometric modeling difficulties and advantages in FEA. In Section 5, they are discussed, validating their results via experimental evidences. Finally in Section 6 the main conclusions are pointed out.

2. Geometric modeling strategies

2.1. Reconstruction from experimental data

Geometric modeling from direct experimental acquisition are usually based on the elaboration of 3D-tomographies via voxel structure. It requires the subtraction from a bulk model of the voxels included in the scanned porosity, as defined through image analysis techniques. In the field of mechanical characterization, it is also associated to the Representative Volume Element (RVE) technique [6]. RVE defines a mesoscale model able to give a global description of the material-discontinuity. When FEA must be carried from the RVE model directly, the choice of the RVE length represents the core of the procedure. In [7], RVE length was related to the reliability of the stress-strain distribution. Because increasing RVE length means reducing the number of nodes, passing from 273×10^3 to 14×10^3 nodes, the error from the experimental value of the Young modulus passes from 28% to 42%, demonstrating a loss of accuracy of the specimen stiffness due to the merge of some voids, whereas the local evaluation of stress at the thicker walls remains the same. RVE is used in bioengineering where the length ratio between meso/macro-scale is of about 1:100-1:50 mm/mm according to porosity volume fraction of 0.30-0.49. Void granulometry from image analysis allows also RVE reconstruction from registered data. It is done in [11] assuming two strategies: in a control volume (e.g. the specimen) RVE is iteratively inserted into blank, if porosity volume fraction is > 0.50, or its voids are subtracted from the bulk, if it is < 0.50. The iterations work from the center of the control volume to the edges. At the end, check and refinement are performed to evaluate the discrepancy from the input porosity volume fraction and the hypothesis on the cell shape (close or open).

Another experimental approach is based on metallographic cross-sections. To obtain a 3D FE model by stacking the cross-sections, some authors use laser scanner acquisitions although also in this case image analysis may allow contour segmentation [8]. Reconstruction process follows a typical reverse engineering process, since the scanned sections are imported as cloud of points in a

CAD environment. After this, in order to obtain the voids, surface reconstruction and stratification are necessary to generate the 3D model. Major problems related to this approach are difficulties in defining the proper height of the cut (impossibility of specimen cutting if the thickness is too small, low resolution of the reconstruction if it is too thick) and in evaluating a systematic workflow to stack the slices, or section, that derives from the cuts. More in detail, the acquisition of the two halves, which are associated to a cut, is able to describe only the cells that pass through that section. Therefore, the cells of the current section must be aligned with the previous one in the respect of the slice stacking constraint. In addition to these problems the processing will also suffer for the intrinsic limit of reverse engineering: data scattering due to noise and bad acquisitions, missing data in case of undercuts. Noise can make hard the alignment between the two halves of one cut, undercut holes requires time to be filled. Moreover, to guarantee surfaces of good quality for the FEA mesh, it will be necessary to post-process one section per time and then proceed to the slice alignment. This causes a loss of efficiency in case of stacking many slices.

2.2. Numerical generation from registered data

Regular cells may be modeled through pattern replication of a basic volume (the cell). It requires the definition of a cell geometry and its subtraction from the component bulk shape according to the required density. The most adopted cells are polyhedric (e.g. Kelvin cell), elliptical or a lattice structure [12]. In this last case, open regular cells are obtained. Although many works are present in literature, for metallic foam characterization, this approach is unable to take into account realistic changes of cell shape, being more adapt for regular cell distributions. To bypass this limit, mixed approaches have been defined introducing probabilistic distribution in a regular cell morphology. Doing so, volume subtraction may build also stochastic cells according to probabilistic distributions related to cell's length and position [1].

Stochastic cell distribution can be modeled also by the so-called Voronoi approach [5]. It is a computational geometry construct related to the space partitioning according to the near-neighbor rule. Each cell can be associated to a point, thus the region of the space, which is the closest to its convex hull, represents the void edge. Many applications are derived from this approach and some of them are also related to RVE applications (for example see [6]) because Voronoi diagram concerns with the geometrical description of the problem. The general procedure consists of defining a Pore Volume Fraction (PVF) so to derive the number of cells (N) that must be included in the specimen volume according to their shape and average dimension (and to the required density). For spherical cells, with radius R, the relation is:

$$PVF = N\frac{4}{3}\pi R^3 \tag{2.1}$$

In this work, the Voronoi approach has been developed in a MATLAB function able to defined N cells, evaluated according to Eqn. (2.1) and randomly distributed in the specimen. PVF is assessed starting from the requested effective density of the foam:

$$PVF = \left(1 - \frac{\rho_{effective}}{\rho}\right) \tag{2.2}$$

Although Eqn. (2.1) assumes spherical voids, the Voronoi diagram of the N seeds defines random shaped cells. Their distribution can be controlled by the assumption of a mean radius, R, or by the effective specimen volume:

$$V_{effective} = V \cdot (1 - PVF) \tag{2.3}$$

where V stands for the specimen's bounding volume.

$V_{effective}$ is correlated to R by the PVF and wall thickness of the cell. In case of uniform wall thickness, t, a first approximation of the effective material volume can be found by:

$$N = floor\left[\frac{V \cdot (1 - PVF)}{0.5\pi \cdot t \cdot R^2}\right] \tag{2.4}$$

Voronoi cells are then generated, through the MATLAB function Voronoi, using N seed points randomly distributed in V. The associated Voronoi diagram is related to the cells' convex hull, without taking into account the wall thickness, t. It is applied by offset, cell by cell approximating a constant thickness. Two constraints have been also applied: (a) the deletion of cells with $R \leq 1.5$ mm, since they are not representative of metallic foam voids (although they may exist, from the structural point of view they are considered as microporosity in comparison of the foam's cells); (b) the cell modification if one or more vertexes are outside V. In both cases the effective PVF is reduced, thus, a correction factor must be multiplied to Eqn. (2.4) and the cell generation becomes iterative since the required tolerance for the $V_{effective}$ is reached.

3. Comparison

Tab. 1 summarizes the documented approaches according to some evaluation criteria related to the necessity of experimental acquisition and the efforts for surface modeling and processing for FEA.

Table 1. Comparison among documented approaches.

	RVE	Reverse Engineering	Pattern Replication	Voronoi Cell
direct from experimental	yes/no	yes	no	no
cell shape	open/close also polyhedral	as experimented	open/close also polyhedral	open/close polyhedral
stochastic	yes	as experimented	no/yes with major efforts	yes
type of model	discrete	discrete/surface	surface	discrete
field of application	bioengineering, mechanical	mechanical	mechanical	multipurpose
post-proc time	medium	high	low	medium
FEA aptitude	good	low	good	medium

Pattern replication can be seen as a solid modeling technique. Its outputs are surfaces and volumes thus the FE models may be derived with minor post-processing (e.g. mid-surfacing in case of shell elements), after neutral format data exchange, e.g. Iges surfaces. On the contrary, major efforts are required in the surface model step to insert stochastic variation of cell distributions, like shape transition from ellipsoidal to polyhedral. Basically, it asks for an iterative procedure to check the effective density obtained and the intersection among cells. In particular, cell intersection must be evaluated to avoid non-manifold or wrong surfaces/edges that can make difficult the FEA meshing step, asking for defeaturing. In addition, to reach high PVF values, thousands of geometric entities must be created. Modeling operations on this high number of elements decreases CAD systems performance, similarly to what happens in CAD modeling of lattice structures made by additive manufacturing [4], [9].

Reverse engineering, intended as derived from point-cloud segmentation and not from voxel reconstruction, is intrinsically laborious because of the 3D nature of the voids. Without reliable automatic segmentation and careful checks of the tessellation quality is rather difficult to achieve good FEA models from the STL file, systematically. The advantage may concern with the capability of reach smooth void shapes, if the resolution of the acquisition is good enough.

RVE and Voronoi cell approaches seem to be the most versatile in terms of cell shape and distribution. In both cases, void surface is discrete. RVE can be automatically associated to a FEA solid mesh, while for the Voronoi cell it can be more difficult. Typically Voronoi output data is an STL triangulation. Although it is a tessellation, shape parameters of many elements are not valid for FEA, both if the model is made by 2D elements (shells) or 3D (tetrahedral). In any case, the surface mesh of the STL file must be optimized. The geometric constraints are the element length and the dihedral angle. Element length must be chosen according to the cell size. Lower values improve cell shape approximation but increase the number of FEA elements, and consequently the computation time. Dihedral angle must be set $\geq 30°$. This value, similarly to the aspect ratio, represents the limit for validity check of a FEA mesh to avoid improper element distortions under loading.

In Fig. 2, an example of all these ideas is given through a Voronoi approach test case, from the seed generation in the specimen V, to the cell surface generation, Fig. 2(a), to the mesh optimization, that is highlighted by zooming a mesh detail of the same voids shown in fig. 2(b).

4. Applications

4.1. Voronoi model

In this work the Voronoi model has been applied on a virtual specimen $60\times60\times60$ mm. It has been built starting from a nominal PVF of 41%, a number of seeds equal to 3261 and a nominal wall thickness of 2 mm. From these input an effective PVF of 25% has been achieved, accepting 2300 seeds in the volume. The effective density has reached 2.05×10^{-6} kg/mm^3, which means a relative density ratio equal to 0.76.

Fig. 3 shows the tessellated surface after optimization obtained with a max element length of 3.6 mm, the frequency histogram of the cell radii and the pseudo-roundness, which has been computed as the ratio between the volume of the cell and the equivalent sphere inside the cell, and an overview of a section after tetrameshing.

The FEA model has been made by 138 000 nodes and 565 000 elements. The analysis has been made through incremental loadsteps applied vertically at the nodes on the top surface, to simulate a compression. Solution has been set as non linear to make possible large displacements and plasticity. Material model has been defined as bi-linear elasto-plastic (yield set at 120 MPa)

Fig. 4 shows the evolution of the vertical displacement up to -10 mm of imposed displacement. These snapshots are referred to a semisection, which has been taken in the

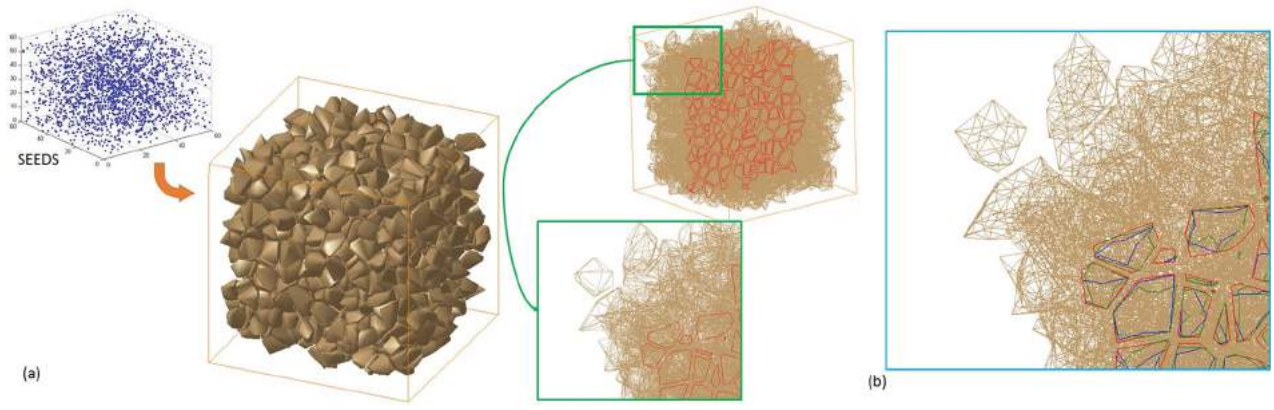

Figure 2. Voronoi approach. (a) Cell generation from seeds; (b) STL optimization.

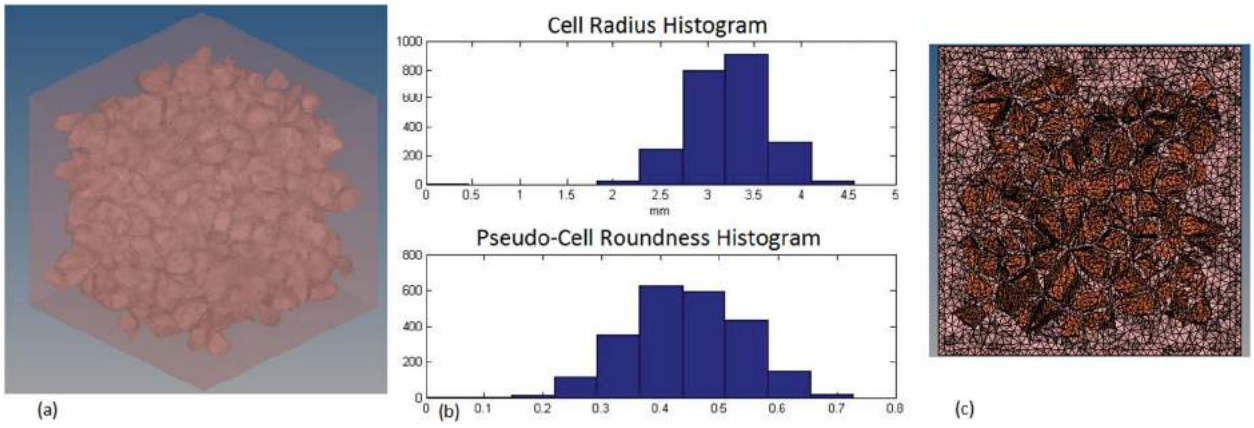

Figure 3. (a) STL final model; (b) cell frequency histograms; (c) tetramesh, section view.

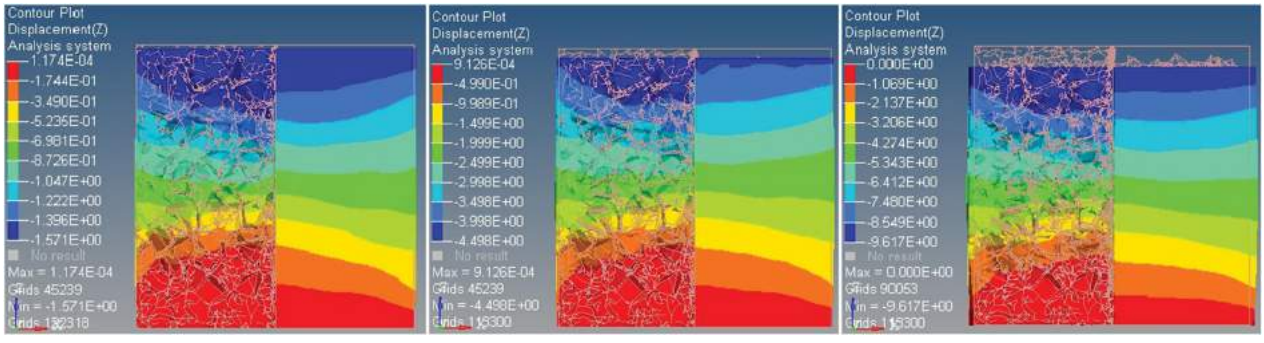

Figure 4. Vertical displacements at three different loadsteps.

middle of the specimen, to see inside the foam, and to the semi front-view (on the right) to see the specimen from the outside.

In Fig. 4 feature edge line of the undeformed shapes have been superimposed. It shows that at the bottom part of the specimen no relevant displacements have been reached since it is near the geometric constraints. Nevertheless inside the specimen the contour plots differ from the outer face's ones. This means that inside the foam a larger volume has not been involved in the deformation instead of the compact faces outside the specimen. This is also confirmed by the stress-strain distribution as shown in Fig. 5. Fig. 5(a) and Fig. 5(b) show the strain contour plots computed at the 7th loadstep in two vertical section taken at 15 and 25 mm from one of the vertical outer face of the specimen. Fig. 5(c) is referred to a section taken at 115 mm where cells become very coarse.

Fig. 6 shows the contour plots of the stress at the 7th loadstep, referred to a 15 mm and 65 mm vertical section, Fig. 5(c) reports a global overview of the stress in the specimen.

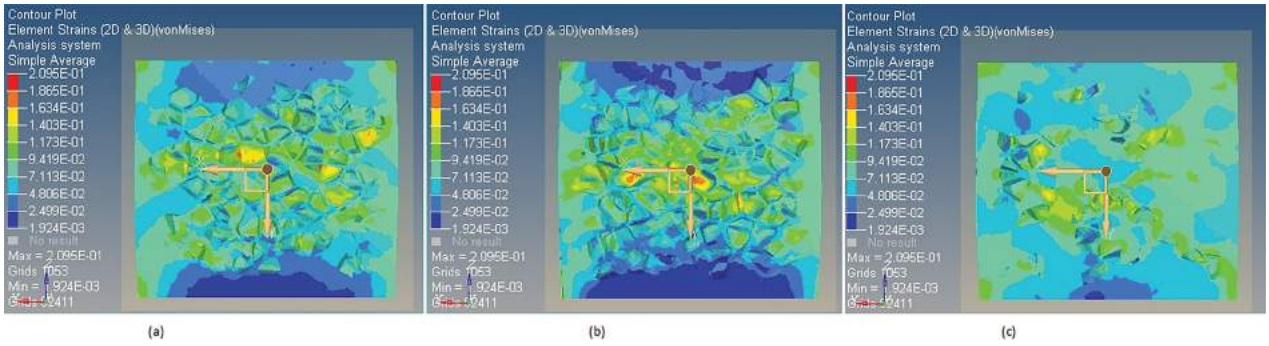

Figure 5. Element strains in vertical sections: (a) @15 mm; (b) @25 mm; (c) @115 mm.

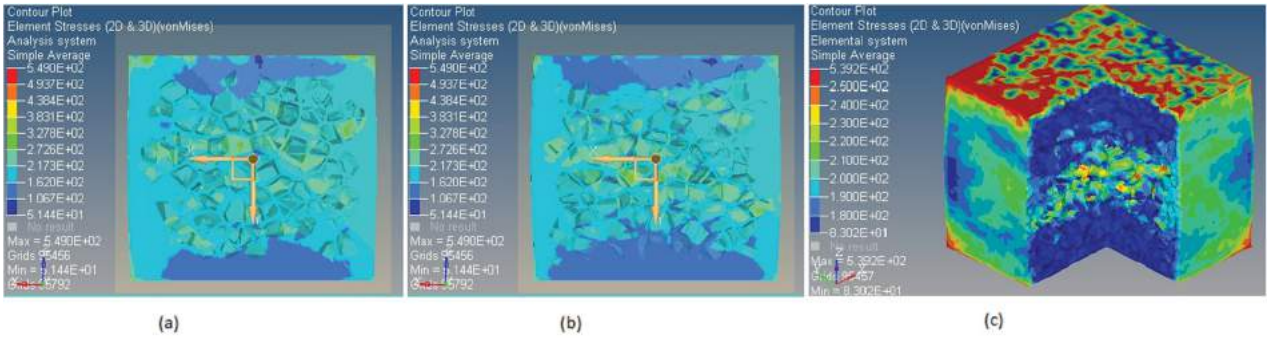

Figure 6. Element stresses: (a) @15 mm; (b) @55 mm; (c) isometric view with sections.

4.2. Reverse engineering

The Reverse Engineering approach has been tested on a subset of points taken from a laser scanner acquisition of the cross-section of an Al7075 specimen, as reported in the box of Fig. 7(a). In this test case, only one half of a cut has been investigated through its cross-section, with the aim of evaluating the operations necessary without taking into account the slice stacking.

The surface reconstruction and modeling have been made starting from the cloud of points represented as iso-level curves in Fig. 7(b). This cloud has been filtered to reduce experimental noise and resampled. Resampling has been used to check, according to a specific tolerance, which points laying on the section. Then, during slice stacking, they are set exactly on the cutting plane to guarantee the coincidence with the second half of the cut.

Fig. 7(c) represents the resample of the area in the detail box of Fig. 7(a) and 7(b), Fig. 7(d) shows the surface triangulation before the hole filling of the undercuts.

To capture cell shapes, 52,000 points have been resampled on a planar surface of 12×13 mm. After hole filling, the 2D STL mesh has been optimized and the volume corresponding to the slice has been derived, assuming a cut height equal to 4 mm, since the maximum depth of the cavities is of about 3.42 mm. Fig. 8 shows the optimized surface mesh and the tetramesh of the half cut derived from it.

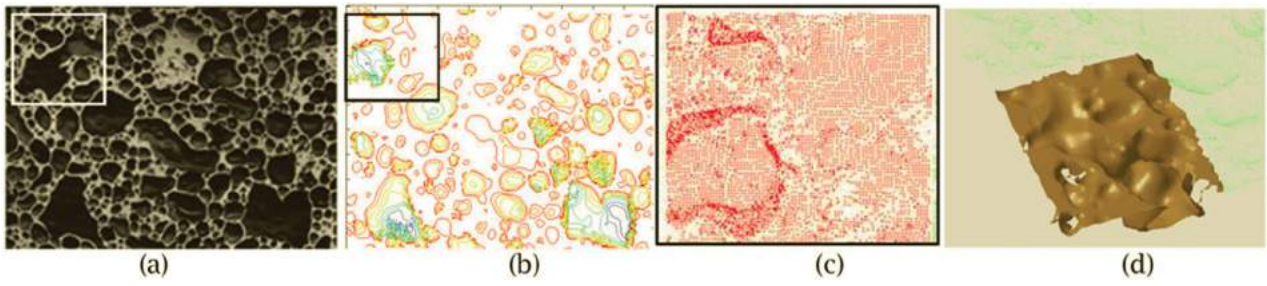

Figure 7. Reverse engineering test case: (a) experimental croos-section; (b) iso-level curves of the acquisition; (c) investigated surface; (d) STL reconstrunction after noise filtering and resampling.

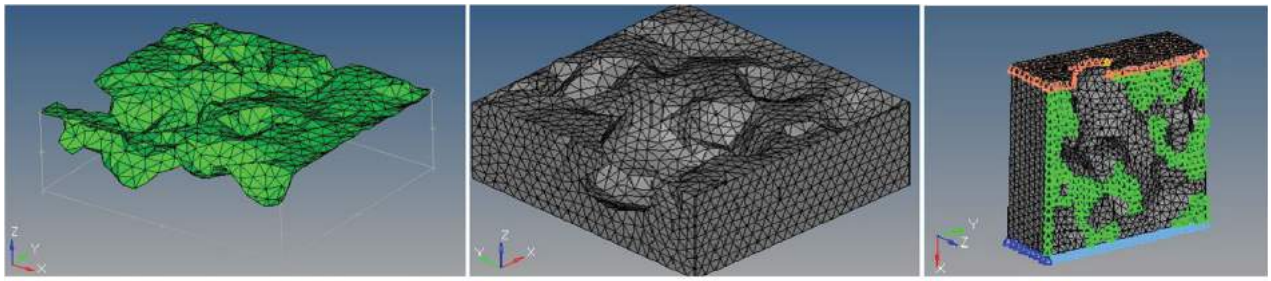

Figure 8. (a) 2D mesh after optimization; (b) tetramesh of the slice; (c) FEA constraints and imposed displacements.

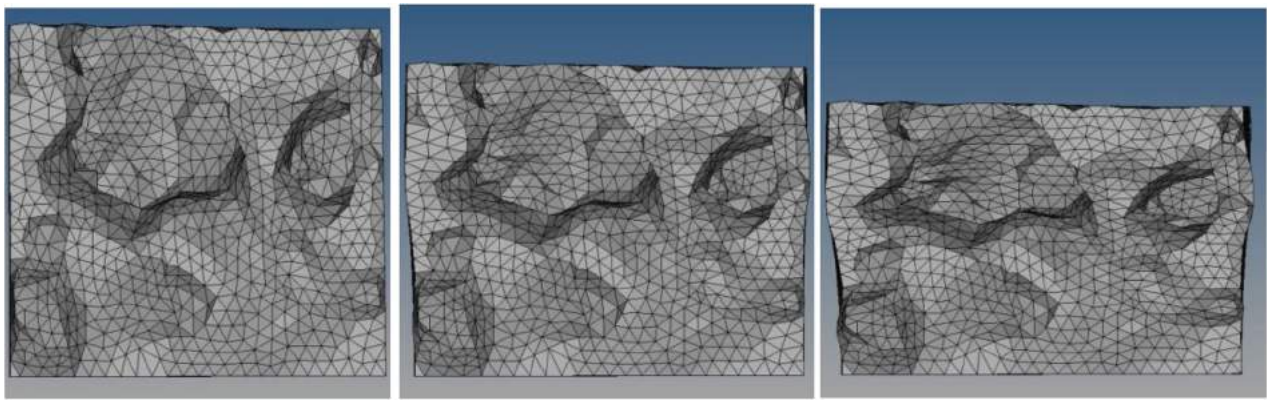

Figure 9. Deformed mesh at 1.5%, 10% and 20%.

The FEA model has 26,980 elements with mesh max element size set to 1.5 mm and aspect ratio to 0.8.

Also in this test case, the solution has been set as non linear to make possible large displacements and plasticity. Material model has been defined as bi-linear elasto-plastic (yield at 120 MPa). To simulate the physical constrain due to the second half cut of the slice, planar symmetry constraints have been applied on the nodes of the cross-section x-y, as shown in green in Fig. 8.(c). In Fig. 8.(c), blue symbols represent the joint constraint to avoid sliding, while the pink ones in the upper face stand for the imposed displacement along positive x direction that represents the compression load applied to the specimen.

Fig. 9 shows the deformed mesh of the cross-section at 1.5%, 10% and 20%. Fig. 10 shows the contour plots of the plastic strains at 1.5% and 20%. Maximum strain reaches about 0.5 mm/mm and its distribution confirms

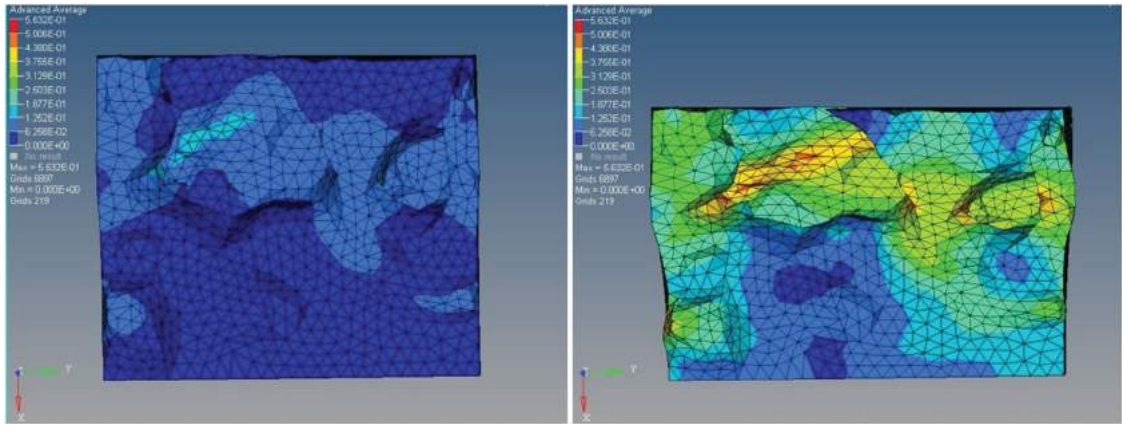

Figure 10. Strain contour at 1.5% and 20%.

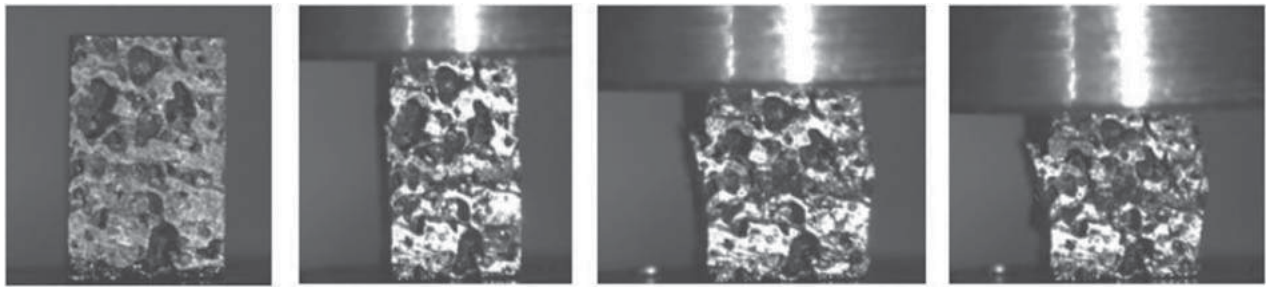

Figure 11. Quasi-static compression test: sequence of deformation.

that the plastic load has been concentrated in the upper cells while the bottom part of the specimen has not been involved in the plastic deformation yet.

5. Discussion

As shown by the contour plots of the two test cases, the mesoscale FEA confirms its capability to describe plastic hinge and the local collapse of cells. In Fig. 11 some experimental evidences of the plastic hinge are given according to a quasi-static test, documented by one of the authors in [3]. The collapse is localized at sections where minimum stiffness is present, not necessary where larger cells are. This phenomenon is present in both the applications, nevertheless the reverse engineering test has been roughly simplified. In fact: (a) only half slice has been investigated, simulating the second one through symmetry constraints on the nodes laying on the cutting plane; (b) just one slice stacking has been done, assuming as bulk material the volume under the acquired surface.

From the cell geometry point of view, obviously, the reverse engineering test case fully accomplishes the reproduction of an Al7075 foams made by metallic powder technology. This process uses TiH_2 as foaming agent of compact powders pre-arranged in dies as semi-finished. It produces closed cells as shown in Fig. 12(a) and Fig. 12(b), surrounded by dense outer walls made by the contact with the die. To give an example of different cell topology, Fig. 12(c) shows the same technology applied to AlSi7, with similar relative density ratio. In this case, the cells are sharper and there is a thicker outside wall.

Considering the Al7075 cell topology, the implemented Voronoi approach gives sharper edges, rather similar to the Alsi7 cells (Fig. 12(c)). Nevertheless in Fig. 12(c) it can be seen that the cell size and distribution is not normally distributed, but it decreases from the centre of the ingot to the outside, according to the temperature cycle determined by the foaming process, as also studied by one of the authors in [2]. Thus, in case of compact powder technology, in the Voronoi approach more sophisticated cell distributions must be implemented to accomplish a more realistic mesoscale CAD modeling. Moreover, some specific check must be defined to calibrate the dense volume near the outer surfaces.

To avoid sharp edges before the mesh optimization, a smoothing process can be made, although it can be insidious since it may involve relevant decrease of the PVF. Specific computation should be made to correct the

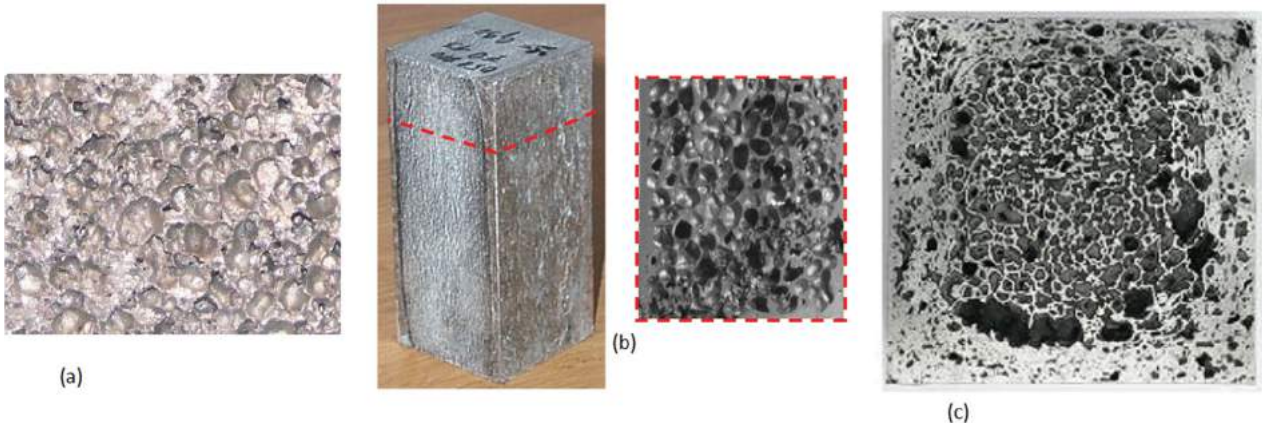

Figure 12. Examples of cell topology (a) and (b) Al7075; (c) AlSi7.

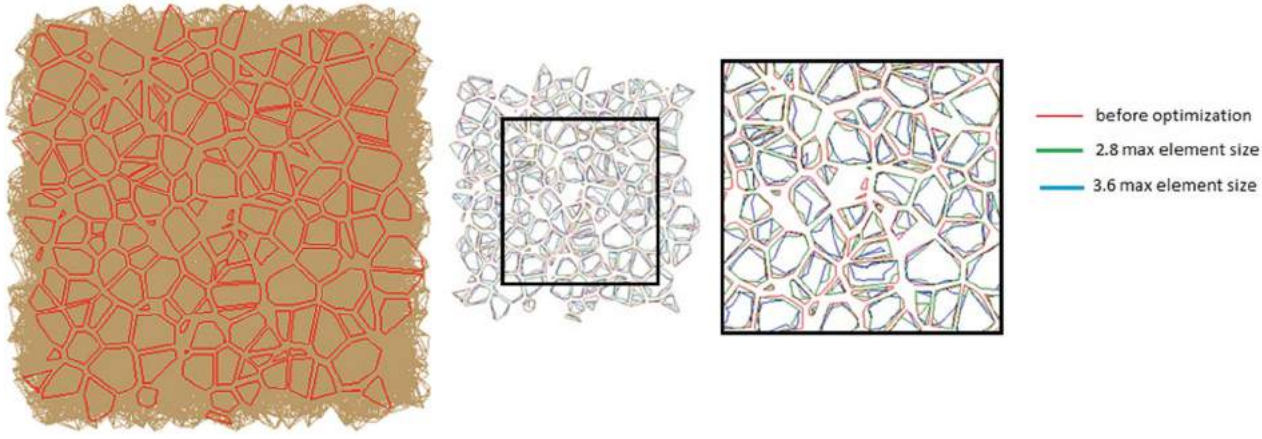

Figure 13. Mesh optimization effect on the cell shape.

initial PVF if cell smoothing are required. Nevertheless a slight smooth effect can be reached by mesh optimization. Fig. 13 shows this effect on the test case of Section 4, in case of two optimized max element length values, 2.8 mm (in green) and 3.6 mm (in blue), red edges represent the initial void shape of the STL file made by the Voronoi implementation.

6. Conclusions

In this work the authors discussed one of the two major problems related to the reliability of FEA in case of cellular materials: the pre-processing phase, or geometric modeling. The second problem, which is not less important than the first one, but beyond the scope of this paper, concerns with the definition of proper constitutive laws and experimental set-up for material characterization.

Here, techniques for geometric modeling of cellular materials has been divided in two fields: the techniques direct from experimental data (tomography or metallographic sections) and those ones based on independent acquired data (e.g. statistical approach by Voronoi diagram). A comparison has been discussed according to the obtained cell topology and post-processing efforts for FEA modeling.

Two tests have been presented to show their aptitude to be used in mesoscale FEA. Both reveals similarity with experimental behavior, confirming the usefulness of mesocale geometric modeling. The test case based on the Voronoi approach, here applied through a specific function developed in Matlab, has been compared to experimental foams made by compact powder technology, highlighting limits and possible enhancement to carry out, in the next, a manufacturing-process-driven geometric modeling technique. Reconstruction and modeling via Reverse Engineering is more time consuming, although it may reproduce cell cavities with better accuracy. Nevertheless efforts must be taken to prepare the cross-section and evaluate the slice stacking.

ORCID

Michele Bici http://orcid.org/0000-0002-7744-2152
Francesca Campana http://orcid.org/0000-0002-6833-8505
Micaela De Michelis http://orcid.org/0000-0002-4662-878X

References

[1] Carofalo A.; De Giorgi M.; Morabito A., Geometric modelling of metallic foams, Engineering Computations, 2013 30(7), 924–935. http://dx.doi.org/10.1108/EC-06-2011-0070
[2] Campana F.; Cortese L; D. Pilone, Property variations in large AlSi7 alloy foam ingots, Materials Science and Engineering A-Structural Materials Properties Microstructure and Processing, vol. 556, 2012, 400–407. http://dx.doi.org/10.1016/j.msea.2012.07.004
[3] Campana F.; Mancini E.; Pilone D.; Sasso M., Strain rate and density-dependent strength of AlSi7 alloy foams, Materials Science and Engineering: A, 2016 651, 657–667. doi:10.1016/j.msea.2015.11.007.
[4] Gibson I., Rosen D.W., Stucker B., Additive manufacturing technologies, 2010, Springer, New York, doi:10.1007/978-1-4419-1120-9.
[5] Gil Montoro G. C.; Abascal J. L. F., The Voronoi Polyhedra as Tools for Structure Determination in Simple Disordered Systems, The Journal of Physical Chemistry, Vol. 97, No. 16, 1993, 4211–4215.
[6] Kanit T.; Forest S.; Galliet I.; Mounoury V.; Jeulin D., Determination of the size of the representative volume element for random composites: statistical and numerical approach, International Journal of Solids and Structures, 40, 2003, 3647–3679. http://dx.doi.org/10.1016/S0020-7683(03)00143-4
[7] Maire E.; Fazekas A.; Salvo L.; Dendievel R; Youssef S.; Cloetens P.; Letang J.M., X-ray tomography applied to the characterization of cellular materials. Related finite element modeling problems, Composites Science and

Technology, 63(16), 2003, 2431–2443. http://dx.doi.org/10.1016/S0266-3538(03)00276-8.

[8] Michailidis N.; Stergioudi F.; Omar H.; Tsipas D.N., 2010, An image-based reconstruction of the 3D geometry of an Al open-cell foam and FEM modeling of the material response. Mech. Mater. 42, 142–147.

[9] Oropallo W., Piegl L.A., Ten challenges in 3D printing, Engineering with Computers, January 2016, Volume 32, Issue 1, 135–148. http://dx.doi.org/10.1007/s00366-015-0407-0.

[10] Simone A.E.; Gibson L.J., Effect of solid distribution on the stiffness and strength of aluminium foam, Acta Mater 1998, 46:2139–50. http://dx.doi.org/10.1016/S1359-6454(97)00421-7.

[11] Simoneau C.; Terriault P.; Rivard J.; Brailovski V., Modeling of metallic foam morphology using the Representative Volume Element approach: Development and experimental validation, International Journal of Solids and Structures, 51(21–22), 2014, 3633–3641. http://dx.doi.org/10.1016/j.ijsolstr.2014.06.027.

[12] Zhang J., The Mechanics of Foams and Honeycombs, Cambridge University Press, Cambridge (UK), 1989.

[13] Zhang C.Y.; Tang L.Q.; Yang B.; Zhang L.; Huang X.Q.; Fang D.N., Meso-mechanical study of collapse and fracture behaviors of closed-cell metallic foams, Computational Materials Science, 79, 2013, 45–51. http://dx.doi.org/10.1016/j.commatsci.2013.05.046.